Titre: Title:	Live streaming of uncompressed HD and 4K videos using terahertz wireless links
Auteurs: Authors:	Kathirvel Nallappan, Hichem Guerboukha, Chahe Nerguizian, & Maksim A. Skorobogatiy
Date:	2018
Type:	Article de revue / Article
Référence: Citation:	Nallappan, K., Guerboukha, H., Nerguizian, C., & Skorobogatiy, M. A. (2018). Live streaming of uncompressed HD and 4K videos using terahertz wireless links. IEEE Access, 6, 58030-58042. https://doi.org/10.1109/access.2018.2873986

Document en libre accès dans PolyPublie
Open Access document in PolyPublie

URL de PolyPublie: PolyPublie URL:	https://publications.polymtl.ca/5051/
Version:	Version officielle de l'éditeur / Published version Révisé par les pairs / Refereed
Conditions d'utilisation: Terms of Use:	CC BY

Document publié chez l'éditeur officiel
Document issued by the official publisher

Titre de la revue: Journal Title:	IEEE Access (vol. 6)
Maison d'édition: Publisher:	IEEE
URL officiel: Official URL:	https://doi.org/10.1109/access.2018.2873986
Mention légale: Legal notice:	©2018 IEEE. Translations and content mining are permitted for academic research only. Personal use is also permitted, but republication/redistribution requires IEEE permission. See http://www.ieee.org/publications_standards/publications/rights/index.html for more information.

Live Streaming of Uncompressed HD and 4K Videos Using Terahertz Wireless Links

KATHIRVEL NALLAPPAN[1,2], **(Graduate Student Member, IEEE),**
HICHEM GUERBOUKHA[2], **(Graduate Student Member, IEEE),**
CHAHÉ NERGUIZIAN[1], **(Member, IEEE),**
AND MAKSIM SKOROBOGATIY[2], **(Senior Member, IEEE)**
[1]Department of Electrical Engineering, Polytechnique Montréal, Montreal, QC H3T 1J4, Canada
[2]Department of Engineering Physics, Polytechnique Montréal, Montreal, QC H3T 1J4, Canada

Corresponding author: Maksim Skorobogatiy (maksim.skorobogatiy@polymtl.ca)

ABSTRACT Taming the Terahertz waves (100 GHz–10 THz) is considered the next frontier in wireless communications. While components for the ultra-high bandwidth Terahertz wireless communications were in rapid development over the past several years, however, their commercial availability is still lacking. Nevertheless, as we demonstrate in this paper, due to recent advances in the microwave and infrared photonics hardware, it is now possible to assemble a high-performance hybrid THz communication system for real-life applications. As an example, in this paper, we present the design and performance evaluation of the photonics-based Terahertz wireless communication system for the transmission of uncompressed 4K video feed that is built using all commercially available system components. In particular, two independent tunable lasers operating in the infrared C-band are used as a source for generating the Terahertz carrier wave using frequency difference generation in a photomixer. One of the IR laser beams carries the data which is intensity modulated using the LiNbO$_3$ electro-optic modulator. A zero bias Schottky diode is used as the detector and demodulator of the data stream followed by the high-gain and low-noise pre-amplifier. The Terahertz carrier frequency is fixed at 138 GHz and the system is characterized by measuring the bit error rate for the pseudo random bit sequences at 5.5 Gbps. By optimizing the link geometry and decision parameters, an error-free (BER $< 10^{-10}$) transmission at a link distance of 1 m is achieved. Finally, we detail the integration of a professional 4K camera into the THz communication link and demonstrate live streaming of the uncompressed HD and 4K video followed by the analysis of link quality.

INDEX TERMS 4K video, broadband communication, streaming media, Terahertz communications.

I. INTRODUCTION

The internet protocol data traffic is continuing its exponential increase and is expected to reach over 278 Exabytes per month by 2021 [1]. Similarly, the ever-increasing wireless communications data rate in the commercial markets is expected to be 100 Gbps within the next 10 years [2]. To meet the bandwidth demand, a shift towards higher carrier frequencies has been considered as a solution [3], [4]. While the carrier frequency below 100 GHz is the immediate solution for high speed wireless applications, the offered data rate is still two orders of magnitude below the expected demand [5]. The availability of several atmospheric transmission windows and broad bandwidth of the channels in the Terahertz (THz)

range (100 GHz-10 THz) is interested to meet the required demand. Therefore, the frequency band above 100 GHz is seen by many as the next frontier in wireless communications [6], [7]. It is worthy to mention that the start of the THz frequency spectrum is not clearly defined whether it begins from 100 GHz or 300 GHz. Some research communities define the start frequency at 100 GHz. Among the important organizations, we note that the International Telecommunication Union (ITU) [8] and Asia Pacific Telecommunity [9] define the beginning of the THz region at 100 GHz. Also, the same organization (ITU) specified 30-300 GHz as millimeter waves in their later report [10]. Since in our work, we used a photonics-based source that can be tuned up to

3 THz, we preferred to refer to our system as a "THz communication system". Recently, the long distance (>2 Km) wireless links operating with a carrier frequency of 120 GHz were reported providing data rates of 10 Gbps and 20 Gbps using amplitude shift keying (ASK) and quadrature phase shift keying (QPSK) respectively [11]–[14].

At the same time, maturing the Terahertz (THz) wireless communication technologies from laboratories into commercial applications is facing multiple challenges. Two major technologies exist in establishing THz wireless communication links: electronics-based frequency multiplier chains and photonics-based frequency difference generation [15]. Electronics-based approaches offer high powers (thus longer link distances), but mainly at lower carrier-wave frequencies (<300 GHz), thus limiting the communication data rates [16]. On the other hand, photonics systems suffer from lower power budgets due to inefficiency in optical to THz conversion, but offer potentially higher data rates at much higher carrier frequencies [15].

From the prospective of telecommunication applications, one of the key advantages offered by infrared (IR) photonics is its ability to interface with the already existing low loss optical fibers for hybrid high speed optical to wireless radio [15], [17]. Therefore, integration of the optics-based THz wireless transmitters with existing IR photonics networks can be done in a seamless fashion. Additionally, high tunability of the THz carrier frequency (between 20 GHz - 3.8 THz [18]–[20]) is easily achievable using photomixing, thus higher carrier frequencies and hence, higher data rates are readily achievable in optics-based THz systems. Recent advances in the uni-traveling carrier photodiodes (UTC-PD) based THz photomixers give a new hope for commercial applications of photonics-based THz communication systems [21]–[24]. Such devices offer relatively high powers (∼1 mW) even at the carrier frequency of 300 GHz [25]. By using a hybrid approach incorporating both UTC-PD as the emitter and solid-state devices such as Schottky diodes as receivers, several high-speed THz communication links have been demonstrated in recent years. Data rates of 48 Gbps at 300 GHz [26] and 50 Gbps at 330 GHz [27] have been achieved in real-time measurements using amplitude shift keying (ASK) modulation of the optical signals. Similarly, using higher order modulation and offline signal processing techniques, 75 Gbps at 200 GHz [28], 100 Gbps at 237.5 GHz [29], 46 Gbps at 400 GHz [30] and 60 Gbps at 400 GHz [31] have been demonstrated. Using multi-channel modulation and single emitter configuration, a higher data rate of 160 Gbps has been reported recently [32]. As a practical application, a few works have shown successful transmission of HD and 4K video in the lower THz band [13], [33]–[37]. Similarly, using photonics based THz emitter and heterodyne receiver operating at 600 GHz, a successful transmission of HD video has been demonstrated over a short range (0.5 m) with a received THz power of 10 nW [38]. All these demonstrations have been carried out mainly using the proprietary components

such as photomixer and without any analysis of the video quality.

With ever increasing wireless data rate, mobile backhaul for transferring large bandwidth signals between base stations and end users is one of the primary targets for using THz band. Employing a highly efficient wireless backhaul service by connecting multiple base stations with small cell size will ensure high data rate to the end users [39]. Thus, enabling photonics based wireless links (millimeter to THz frequency band) offers high efficiency and cost-effective solution to the mobile backhauling and 'last mile' connections [40], [41]. Similarly, the THz communication systems can be used to establish short range high-speed wireless links for applications such as chip-to-chip communications, KIOSK downloading, high-speed indoor wireless LAN to name a few [42].

Among several bandwidth hungry applications, wireless transmission of uncompressed HD, 4K and 8K video finds importance in applications such as education, entertainment, telemedicine, security, video conferencing to name a few. It is reported that the market value of 4K technology will reach $102.1 billion by 2020 [43]. Wireless streaming of high quality videos is already used in biomechanical analysis, unmanned aerial vehicle (UAV) unmanned ground vehicle (UGV) and telemedicine. In biomechanics, by transmitting the uncompressed video content wirelessly to a remote workstation, the motion analysis (sports person for example) can be performed in real-time [44].

In telemedicine, transmission of HD video from the remote location (ambulance for example) to the hospital, a hybrid optical-wireless technology with low latency would be the ideal solution [45]. An unprecedented level of detail to judge the patient condition can be inferred from the video using a zoom-in feature with uncompressed 4K or 8K cameras at the remote pre-medical center [46]. For such applications, a highly efficient beamforming technique is essential while using higher carrier frequency to minimize path loss and to avoid missing of communication between high speed vehicles and base station. Furthermore, the wireless streaming of uncompressed 4K video is of great importance in broadcasting, surveillance, security and ground mapping applications. For example, NHK (Japan broadcasting corporation) has already started trial experiments by telecasting 8K video using proprietary devices for Olympic games that to be held in 2020 [47]. All of the above-mentioned examples suggest that transmission of the uncompressed 4K/8K videos can provide a significant improvement to a variety of important applications in the academics and industries.

Recent developments of hardware components in the THz band promise several game-changing applications. Thus, in this article, encouraged by the recent advances in the THz and IR photonics, we show the possibility of assembling a high-performance THz communication system for real-world applications, by borrowing off-the-shelf commercial components from various communication technologies. We present the design and the performance evaluation of the photonics-based THz communication system that is built using all

commercially available system components. Although several research groups have demonstrated the wireless transmission and display of uncompressed HD and 4K videos, in this work, in addition to the use of all commercial components in building the communication system, we detail the integration, record and analyzed the synchronization error of each frame over long recording duration (30 minutes) for both uncompressed HD and 4K video signals. The paper is organized as follows. Section II presents the experimental setup for the photonics-based THz communication system followed by the characterization of the communication system components in Section III. Section IV presents the Bit error rate (BER) measurement results and finally Section V shows the integration and demonstration of wireless transmission of the uncompressed HD and 4K video streams.

II. TERAHERTZ COMMUNICATION SYSTEM

The schematic of the photonics-based THz wireless communication system is shown in Fig.1. One of the two laser beams is intensity-modulated and then amplified using the Erbium-doped fiber amplifier (EDFA). The laser beams are combined using the 3 dB coupler and then injected into the photomixer for THz generation.
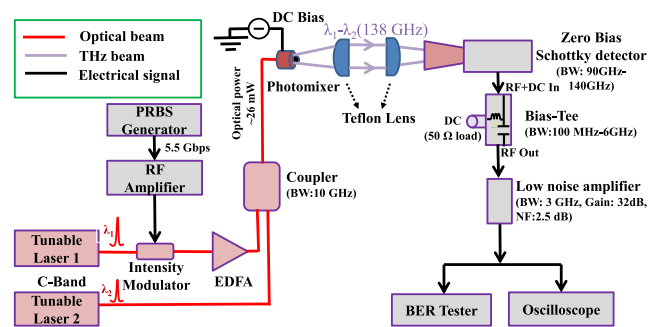

FIGURE 1. Schematic of the photonics-based THz wireless communication system. (EDFA: Erbium doped fiber amplifier, BW: Bandwidth, NF: Noise figure).

In the receiver side, a zero-bias Schottky diode (ZBD) is used to detect and directly demodulate the incoming THz signal. The DC field present in the demodulated baseband signal is filtered using Bias-Tee and amplified using a low noise amplifier (LNA) for further signal processing. The components of the THz communication system are detailed in what follows.

A. LASER SOURCE

Two tunable distributed feedback (DFB) laser diodes operating in the C-band (Toptica Photonics) with an output power of ∼30 mW each are used to optically drive the THz emitter. The linewidth of each laser is ∼0.5 MHz on a short time scale (100 μs), while the laser frequency may drift over a few tens of MHz in a few minutes depending on the stability of the ambient conditions. Both diodes are mounted in a compact laser head and the output beams are delivered via a polarization-maintaining (PM) single-mode fiber. The

wavelength tuning behavior of the lasers is calibrated [48] and the output THz frequency -i.e., the frequency difference of both lasers- is tuned using an Field Programmable Gate Array (FPGA)-based control module ("Teracontrol" by Toptica Photonics which controls the lasers thermally using temperature and current controller).

B. DATA MODULATION

One of the lasers is intensity-modulated (Amplitude shift keying modulation, ASK) using an external electro-optic Mach-Zehnder modulator (MZM) (Thorlabs-LN81S-FC). The typical insertion loss and pseudo random binary sequence (PRBS) optical extinction ratio of MZM are 4 dB and 13 dB respectively. The input signal to the MZM is split into two arms and combined at the output port. The amplified RF signal is connected to one of the arms which changes the refractive index of the substrate resulting in either constructive or destructive interference at the output port, resulting in the modulation of optical beam. The operating bias point of the modulator is controlled by the modulator driver unit (Thorlabs-MX10A) which also acts as an RF amplifier and optical attenuator. The modulator is locked to the quadrature bias point with positive slope which is monitored continuously using a dither tone to detect and correct any drift in the bias voltage. The frequency and amplitude of the dither tone is set to 3 KHz and 600 mV$_{pp}$ respectively. The THz communication system is characterized by transmitting the Non-Return to Zero (NRZ) PRBS data which is generated by the pulse pattern generator (PPG) unit integrated in the test equipment (Anritsu-MP2100B). The generated PRBS data with a peak-to-peak amplitude of 0.4 V$_{pp}$ is connected to the modulator driver unit while the amplified electrical data with amplitude of 5 V$_{pp}$ is fed to the optical modulator. The optical output power after the electro-optic modulator is ∼200 μW and is fixed to a constant of 110 μW using the variable optical attenuator to avoid any power fluctuations during the experiments. It is further amplified using EDFA amplifier (Calmar laser-AMP-PM-18) to ∼13 mW. The pump current of the EDFA is adjusted to have an average output power similar to the unmodulated direct laser beam.

C. THz GENERATION

A 3 dB fiber coupler is used to combine the direct and modulated laser beams and the output is fed to the photomixer (Toptica Photonics) for THz generation. The photomixer features a silicon lens (6.05 mm ± 0.1 mm thickness and 10.0 ± 0.1 mm diameter) to pre-collimate the output THz beam. The gain of the photomixer is contributed by both structure of the antenna (Bowtie) and silicon lens which is ∼17 dBi and ∼19 dBi at the carrier frequency of 100 GHz and 140 GHz respectively [49]. The Teracontrol module is also used as the DC voltage source to drive the photomixer electrically. The output THz power of a photomixer is shown in Fig.2, which is measured using calibrated Golay cell [50]. We see that the output power is not uniform and the high power is obtained mostly below 200 GHz. Two plano-convex
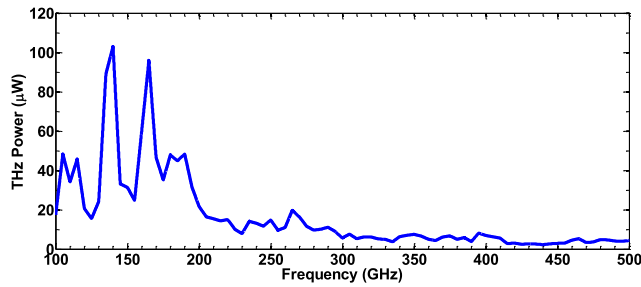
FIGURE 2. THz output power from the photomixer measured using a calibrated Golay cell with 5 GHz spectral resolution (Courtesy of Toptica Photonics).

FIGURE 4. Estimate of the maximal voltage at the ZBD's output when used with Toptica's THz photomixer. Grey areas correspond to the THz atmospheric transmission windows as identified in [48].

lenses (Thorlabs-LAT100) with a focal length of 100 mm and a diameter of 50 mm are used to collimate the THz beam in free space and focus it again into the detector.

D. THz DETECTION AND DEMODULATION

A ZBD with a horn antenna is used to detect and demodulate the incoming THz signal. The choice for the THz carrier frequency is determined by the product of the output power of the THz emitter and the responsivity of the ZBD. Particularly, two ZBDs (Virginia diodes WR8.0ZBD-F and WR6.5ZBD-F) with a working range below 200 GHz were used in the analysis. The responsivity data for both detectors is shown in Fig.3.
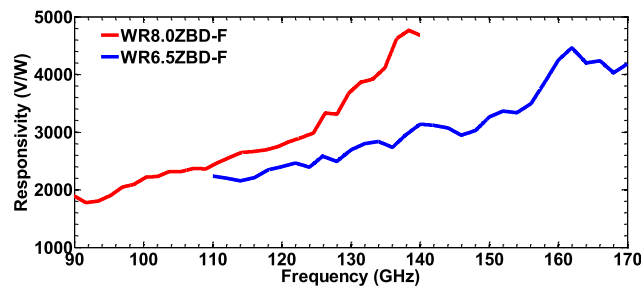

FIGURE 3. Responsivities of commercial ZBD's WR8.0ZBD-F and WR6.5ZBD-F (Courtesy of Virginia Diodes).

The maximal voltages at the output of the two ZBDs are estimated by multiplying the emitted THz power as presented in Fig. 2 by the responsivity of a corresponding ZBD presented in Fig. 3. In Fig. 4, we plot such voltages as a function of the THz frequency and conclude that WR8.0ZBD-F ZBD with the conical horn antenna (Virginia diodes WR8.0CH) operating at 138 GHz results in the maximal detected signal amplitude for a back-to-back emitter/detector arrangement. This conclusion was also confirmed experimentally by performing a frequency sweep and detecting the frequency of maximal detected signal at a fixed short link length of ~30 cm. Furthermore, this frequency lies in the second atmospheric transmission window above 100 GHz [51] (grey area in Fig. 4), making it a natural choice as a carrier frequency for THz communications.
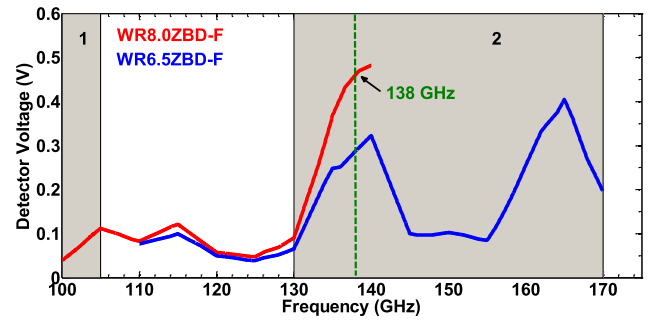
Finally, after ZBD, a Bias-Tee (Minicircuits-ZFBT-6GW+) is connected in sequence to block the DC voltage and let only the AC signal from 100MHz to 6 GHz passing to the next stage. Followed the Bias-Tee, a high gain (>32 dB) and low-noise amplifier (Fairview Microwave-SLNA-030-32-30-SMA) is used to amplify the demodulated baseband signal. The noise figure and the bandwidth of the low noise amplifier (LNA) are 2.5 dB and 3 GHz respectively. The typical output third order intercept point of the LNA is +29 dBm.

III. CHARACTERIZATION OF THE COMPONENTS USED IN THE COMMUNICATION SYSTEM

A single-ended, NRZ, PRBS data with a bit rate of 5.5 Gbps and a pattern length of 2^{31}-1 is used as the test signal to characterize the THz communication system. The peak-to-peak amplitude of the test signal is set to 0.4 V_{pp}. The optical spectra of the DFB lasers (before and after modulation) with a frequency separation of 138 GHz are measured using the Optical spectrum analyzer (Anritsu-MS9740A) with a spectral resolution of 0.03 nm as shown in Fig. 5. As discussed in the previous section, one of the lasers is intensity modulated and amplified using the EDFA. First, the PRBS data is turned OFF and the optical output power from the modulator is measured. We observe a high-power loss (>10 dB) due to the optical modulator. The output from the optical modulator is connected again to the modulator driver unit, where the adjustments of the final output power can be done using
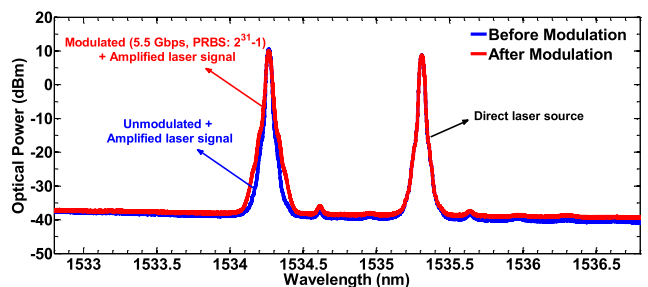

FIGURE 5. Spectra of the input optical signal injected into the THz photomixer. The SNR of >40 dB is achieved.

variable optical attenuator based on user requirement. It is possible to choose either constant output power or constant attenuation mode. We used constant output power mode to avoid any fluctuations in the optical power. Since the optical power from the modulator is low (∼200 μW), we fixed the variable optical attenuator to provide the constant output of 110 μW to further reduce the risk of power fluctuations.

Next, an EDFA is used and by adjusting its pump current, the amplitude of the laser beam is kept similar to that of the direct laser beam (blue curve in Fig.5 pointing unmodulated + amplified laser signal). When two laser beams (modulated and direct laser beam) of equal power (within the damage threshold limit of the photomixer which is ∼35 mW) is mixed in the photomixer (heterodyning) a higher THz amplitude was observed. When the PRBS data is turned ON, the laser beam is now modulated, and we observe an increase in the bandwidth of the modulated laser signal as well as the optical noise floor (∼1 dB) when compared with the unmodulated laser beam as shown in Fig.5 (red curve pointing modulated + amplified laser signal). However, a signal-to-noise ratio (SNR) greater than 40 dB is achieved after the modulation of optical beam (at the input of photomixer) which is recorded by measuring the peak amplitude and noise floor of the laser signal using optical spectrum analyzer. The total optical input power (combined laser power) injected into the THz photomixer is ∼26 mW.

At the receiver side, the Bias-Tee (operational bandwidth 100 MHz - 6 GHz) acts as a band-pass filter as well as to block the DC voltage passing to the next stage (LNA) and thereby to increase the performance. Although the LNA is AC coupled, we observe the improved performance while using the Bias-Tee. The circuit of the Bias-Tee consists of a capacitor and inductor connected in parallel with three external ports (RF+DC-input, DC and RF-output). The connection of Bias-Tee is shown in Fig.1. The DC port of the Bias-Tee is connected to a 50Ω load. Without Bias-Tee, the demodulated baseband signal with floating voltage values passes to the next stage (LNA) minimizing the performance. By connecting the Bias-Tee in between the ZBD and LNA, the floating voltage signals from the ZBD is adjusted to a common reference ground and thereby improves the performance with slightly higher eye amplitude.

To ascertain the impact of the Bias-Tee on the signal quality, an eye pattern is recorded after the LNA using a high-speed oscilloscope (Anritsu-MP2100B) without and with Bias-Tee as shown in Fig.6. The link distance and the DC bias voltage of the photomixer are fixed at 1 m and −1.9 V respectively for this measurement. The eye pattern measured using the Bias-Tee shows higher eye (opening) amplitude (∼18% increase) when compared to the eye pattern taken without Bias-Tee. While it improves the performance of the communication system by blocking the DC voltage, at the same time the Bias-Tee might cause some problems when transmitting almost constant bit patterns (like long continuous string of ones or zeros). This is related to the fact that the low frequency components present in the long continuous
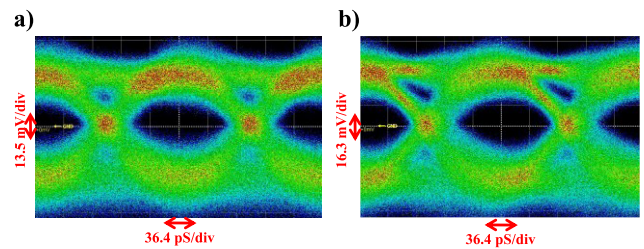

FIGURE 6. Eye patterns for the test signal (PRBS: 5.5 Gbps, 2^{31}-1), a) without Bias-Tee and b) with Bias-Tee.
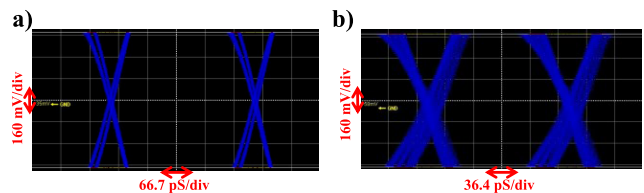

FIGURE 7. Eye patterns from the output of the analogue LNA using digital a) 3 Gbps and b) 5.5 Gbps signals.

pulse are filtered out by the Bias-Tee. For example, the lowest non-zero frequency component present in the PRBS test signal with a bit rate of 5.5 Gbps and a pattern length of 2^{31}-1 is 2.56 Hz ($5.5 \cdot 10^9 Hz/2^{31}$) and it is filtered out by the Bias-Tee along with its harmonics up to 100 MHz, affecting the quality in the signal reconstruction. While keeping in mind potential issues with long constant bit patterns, we nevertheless observe that using Bias-Tee generally leads to higher performance in our experiments. Because of the lower responsivity values of ZBD's (∼2000 V/W) in the THz region, the corresponding output voltage from them after THz detection and baseband signal demodulation is also lower depending on the received THz power. To amplify the baseband signal, a digital amplifier with broad bandwidth (∼10 GHz for data rate of ∼10 Gbps), low noise-figure (<3 dB), high gain (>30 dB) and SMA connectors (since ZBD's are terminated with SMA connectors) is preferred. To the best of our knowledge, such amplifiers satisfying all the above requirements are not available in the commercial market. Therefore, we used a LNA that is designed for analogue signals in our communication system. However, it can still be used for digital signals.

To test the use of analogue LNA with digital signals, the peak-to-peak amplitude of the test signal is attenuated using a fixed attenuator to ∼30 mV$_{pp}$ in order to protect the test equipment from the damage after amplification (damage threshold of electrical oscilloscope is ±2V). The evaluation of the waveform such as jitter and eye crossing are automated in the test equipment. The RMS jitter of the digital test signal after attenuation (but before LNA) was measured to be 1.28 pS and 1.48 pS for 3 Gbps and 5.5 Gbps respectively. The attenuated digital test signal is then given as the input to the analogue LNA.

The measured eye pattern from the output of the LNA is shown in Fig.7. The RMS jitter measured after the LNA is
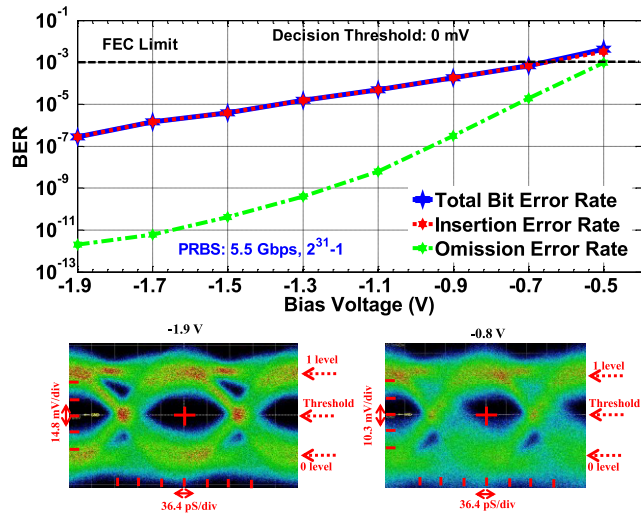
FIGURE 8. Measured BER as a function of the photomixer bias voltage for the PRBS test signal with 5.5 Gbps bit rate and 2^{31}-1 pattern length.

FIGURE 9. Measured BER as a function of the angle θ between the detector and the THz signal propagation direction for the PRBS test signal with 5.5 Gbps bit rate and 2^{31}-1 pattern length. Inset: schematic of the experiment.

4.23 pS and 6.74 pS for 3 Gbps and 5.5 Gbps respectively. Similarly, the eye crossing percentage of the digital signal after the LNA deviates from ideal 50% to ∼48% and ∼40% for 3 Gbps and 5.5 Gbps respectively after amplification. This may be due to the fact that the duration of digital 0 is longer than digital 1 causing the reduction in the eye crossing percentage from the ideal value. Therefore, we conclude that while analogue LNA can be used for amplification of the digital signals, it can also significantly increase the timing jitter and deviation in the eye crossing percentage in the system while increasing the bit rate.

IV. EVALUATION OF THZ COMMUNICATION SYSTEM USING BER MEASUREMENTS

The performance of the THz communication system was then characterized using Bit Error Rate (BER) tester (Anritsu-MP2100B). The BER was first characterized as a function of the photomixer bias voltage, which is a key parameter that defines the emitted THz power. To record a highly consistent BER data in short measurement duration, we choose the target BER of 10^{-12} in our experiments. For the target BER of 10^{-12}, and the bit rate of 5.5 Gbps, the duration of a single measurement is calculated as measurement duration = 1/(target BER * bit rate) ≈ 182sec. The THz output power from the photomixer is proportional to the illuminated optical power and applied bias voltage. By fixing the link distance to 100 cm, illuminated optical power to 26 mW and the decision threshold to 0 mV, the BER was measured after the LNA by varying the DC bias voltage of the photomixer (Fig. 8). The damage threshold limit of the DC bias voltage for the THz photomixer is −2 V and therefore we limited our measurements to a maximum bias of −1.9 V. The lowest BER of ∼10^{-7} was achieved for the bias voltage of −1.9 V.
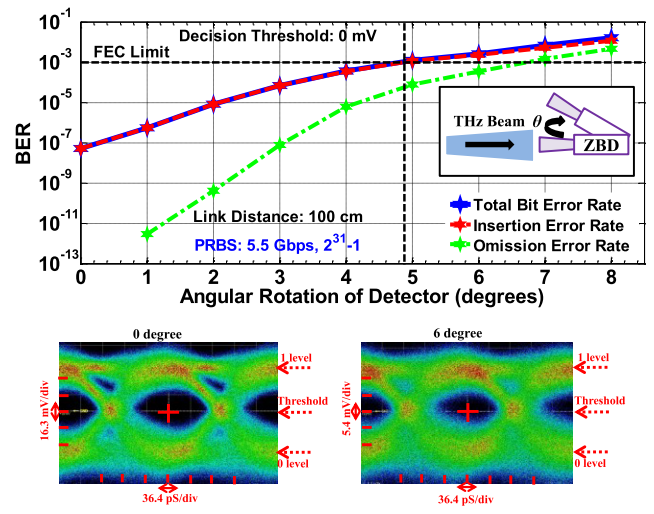
By gradually decreasing the bias voltage, it was found that the BER increased exponentially fast. At the limit of the Forward Error Correction (BER ∼10^{-3}), the bias voltage was −0.7 V. From Fig. 8 we also observe that insertion errors (digital 0 is mistaken for the digital 1) contributes more to the total BER when compared to the omission errors (digital 1 is mistaken for the digital 0). This is due to the vertical asymmetry of the eye pattern in the received signal. The vertical asymmetry in the eye pattern arises from the optical modulation itself. The DC bias to the modulator is locked to the quadrature point (positive slope) of its transfer function. A small uncertainty in the eye amplitude could be due to the minor variation in the DC bias from its ideal position. This is especially pronounced when the data rate is greater than 2 Gbps. As seen from the eye patterns (insets in Fig. 8), the digital 0 is closer to the decision threshold than digital 1, which gives rise to the higher insertion error rate.

Next, we have characterized BER as a function of several communication link parameters such as link distance, as well as angular deviation of the detector antenna from the principal direction of signal propagation. Thus, in the first experiment, we have fixed the link distance of 100 cm and the photomixer DC bias voltage to −1.9 V. The BER was then measured by varying the alignment angle of the ZBD detector antenna with respect to the signal propagation direction as defined by the emitter antenna (see the inset in Fig.9). Experimentally this was accomplished by changing the angle of rotation using high precision rotation mount (Thorlabs-PR01), where the detector antenna is fixed on top of it. The amount of THz power coupled into the detector antenna reduces with increased angular rotation which results in higher bit errors. The total BER was found mainly due to the insertion errors (see Fig. 9) due to asymmetry of the eye pattern in the vertical direction. From these measurements, we found that in order

to stay within the FEC limit, the detector has to be within ~4.8 degrees of the principal beam propagation direction.

In the second experiment, the BER was measured as a function of the link distance. While evaluating the impact of the link distance, the bias voltage and the angular deviation of the detector antenna was set to −1.9 V and 0 degree respectively. First, we fixed the decision threshold to 0 mV and measured the BER at several link distances. As our system was mounted and aligned on the optical table, the measurements were limited to 175 cm long links. The measured BER is shown in Fig. 10 (a), we note that even at 175 cm link length, the total error is below the FEC limit. Due to vertical asymmetry in the eye diagram, the insertion error is again much higher than the omission error. This asymmetry can be addressed by adjusting the value of the decision threshold in order to equalize the insertion and omission errors, which also leads to the lower total BER.
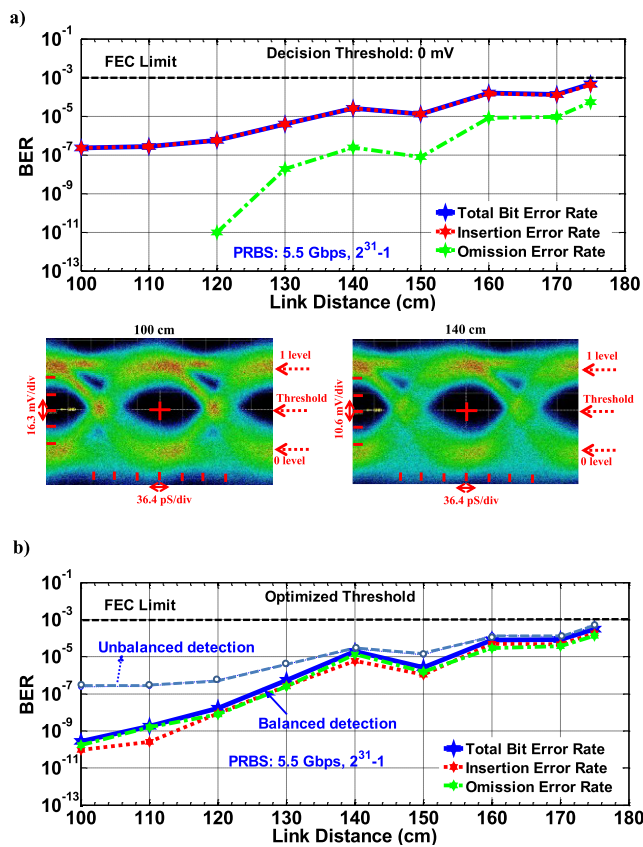

as a function of the link distance, where omission and insertion errors are balanced. For comparison, in the same figure we present total error of the unbalanced system (same as Fig. 10(a)) and note that decision threshold optimization indeed reduced the total BER, which is especially pronounced at shorter link lengths.

In passing we note that for shorter communication links, the main reason for the BER increase with the link distance is divergence of the THz beam, and a consequent reduction of the THz power at the detector site. Particularly, due to diffraction of the collimating lens, the diameter D_{THz} of the THz beam as a function of the link distance L can be approximated as $D_{THz} \sim L \cdot \lambda_c / D_l$, where λ_c is the wavelength of THz carrier wave, and D_l is the lens diameter. If two identical lenses are used to collimate the THz beam and focus that beam onto a detector, then with P_0 power emitted by the photomixer, only $P = P_0 (D_l/D_{THz})^2 \sim P_0 \left(D_l^2 / (L \cdot \lambda_c) \right)^2$ will arrive to the detector. From this we conclude that two strategies can be pursued in order to increase power budget in case of short communication links. These include either using collimating lenses of larger diameter D_l, or using higher THz carrier frequencies (lower λ_c). Although increasing the carrier frequency can lead to less divergence, it can lead to higher path-loss. The path loss mainly occurs due to material absorption (in case of signal passing through the material), diffraction (due to opaque obstacles) and multipath (signal travelling from different paths to reach the receiver). Therefore, the path loss increases with increase in the frequency reducing the power budget. However, for line of sight communication as we demonstrated in this work, the effect of path loss is minimal. For longer communication links, THz absorption in atmosphere becomes important, which further decreases the power budget and increases detection errors.

Now, we discuss several ways to increase the performance and application of the proposed system. Although the electronic based THz communication system can easily reach kilometer link distance, the short communication link distance and the data rate using a photonics approach can be improved by several folds by changing the critical components such as high performance photomixer and LNA. A waveguide integrated UTC-PD photomixing antenna (NTT Electronics) offers output power of ~−5 dBm at 140 GHz can be used. On the other hand, if the power of the THz source is higher, one can take advantage of using commercial broadband digital LNA's with gain less than 30 dB and noise figure greater than 3 dB (products from SHF communication technologies for example). Similarly, multi-carrier modulation along with switching of carrier frequency has no equivalent in electronics-based approach [15]. Although the electronics-based approach is less expensive compared to the photonics-based THz system, the cost can be scaled down commercially by fabricating dual lasers with modulator on a single chip associated with mass production of photomixers. In Table 1, we compare the THz wireless communication systems based on photonics approach in the 100-250 GHz range.

FIGURE 10. Measured BER as a function of the communication link length for the PRBS test signal (5.5 Gbps, 2^{31}-1). (a) Unbalanced system, the decision threshold is fixed at 0 mV. (b) Balanced system: for each link length, the decision threshold is optimized to balance the insertion and omission rates.

Therefore, in the follow-up experiment we optimized the system performance by finding the optimal value for the decision threshold at each link length in order to equalize the insertion and omission errors. In Fig. 10 (b) we plot performance of the optimized THz communication system

Data rate (Gbps)	Frequency (GHz)	Distance (m)	Modulation	Ref.
440	37.5 & 100	1.5 & 0.7	QPSK	[52]
10	120	5800	ASK	[13]
1	146	0.025	ASK	[53]
11	200	0.18	ASK	[54]
75	200	0.02	QPSK	[28]
100	237.5	20	QPSK	[29]
5.5	140	1.75	ASK	This work

In [28], [29], and [52], higher data rates were easily achieved by using higher order modulation schemes (Quadrature phase shift keying-QPSK). In [53], the wireless transmission was demonstrated using a monolithically integrated dual laser to reduce the phase noise and in [54] coherent detection scheme was employed. In [13], a longer link distance of 5.8 km was achieved by proprietary UTC-PD photomixer antenna combined with the Indium phosphide high electron mobility transistor (HEMT) millimeter wave monolithic integrated circuit (MMIC).

The link distance and the data rate are comparatively low in our demonstration, which is due to the low output power of the photomixer. However, the methodology for building a long link communication system is the same. By replacing the low power photomixer with a high power photomixer (~mW), we could readily reach up to 100s of meters and the distance would mainly be limited by the divergence of the beam which requires large collecting optics (eg. large dish antenna). The increased link distance will be sufficient to cover the end users within the femto cell to near pico cell range. In the receiving electronics, by using a high gain amplifier (>30 dB) with broad bandwidth (~15 GHz) and low noise figure (<3 dB), the data rate up to 10 Gbps could be easily reached using the basic ASK modulation. By replacing the intensity modulator with a high bandwidth phase modulator and by employing higher order modulation schemes,

the data rate could be readily improved to few 10s of Gbps. The performance of the system could be further improved by locking the free running independent lasers to a common reference or by using dual lasers fabricated on a single chip. By implementing all the above modifications, the proposed system architecture is greatly suitable for practical applications.

We would like now to comment on the advantages of the system that we have presented in this work. First, the system was assembled by using all commercial components. It means that the result is reproducible and interesting to readers who want to build their own THz communication system. Second, on top of only displaying the wirelessly received video, we also detailed the integration of the communication system to a professional 4K camera along with the required computer configuration for recording and processing the high resolution uncompressed video content (see section V). Therefore, the proposed system can be used in the nuclear power plants for example, which demand wireless transmission of high resolution video content from many nearby inaccessible areas. Another interesting application of the developed communication system is to characterize the THz integrated components and devices such as waveguides, metamaterials, to name a few. Even with the short communication link system, it is possible to experimentally validate several designs of low loss THz waveguides for real-time signal processing. Multiplexing schemes such as frequency division multiplexing, spatial division multiplexing can be studied to increase the channel capacity of the system. Further, with minor modifications in the proposed optical-THz system, several higher order modulation algorithms, multi-carrier modulations (by adding another laser line for example) can be investigated. Beamforming is one of the primary requirements for next generation wireless communication system due to line of sight links. Such techniques using optical phase shifters and new novel materials can be studied using the short communication link photonics-based THz communication system. As the DFB laser can be easily tunable, characterization of the wireless channel (indoor) over a wide frequency range from 50 GHz to 3 THz (using antenna integrated photomixers at both transmitter and receiver) can be performed. Also, by using widely tunable THz system it is possible to experimentally study various THz sensors and THz imaging algorithms. As said, either by using the proposed design directly or with minor modifications, it is possible to address several applications in both academics and industry.

V. TRANSMISSION OF UNCOMPRESSED HD AND 4K VIDEOS USING THZ COMMUNICATIONS

As indicated in the introduction, one of the important practical applications of THz communications is wireless transmission of high-quality video. In what follows, we first detail integration of the professional 4K camera into the THz communication system detailed earlier, and then demonstrate successful transmission of the uncompressed HD and 4K videos at 60 frames per second (fps) and 30 fps respectively.

Additionally, we discuss two different strategies for the integration of 4K cameras at the transmitter side of a THz communication system depending whether electrical or optical outputs of the camera are used.

A 4K camera (Blackmagic studio camera) with a wide-angle lens (Olympus M. Zuiko Digital ED 12-40mm f/2.8 PRO Lens) was used in our experiments. The camera was equipped with two output ports (optical and electrical). The standard output from a 4K camera is an uncompressed video with 10-bit color depth and Chroma sub-sampling of 4:2:2. The peak-to-peak output voltage from the SDI (Serial Digital Interface) electrical cable is 800 mV$_{pp}$. In Fig.11 (a) we present integration of a 4K camera with THz transmitter when using electrical output from the camera. The electrical cable from the 4K camera has a BNC connector with an impedance of 75Ω, whereas the RF amplifier present in the optical modulator driver has a SMA connector with an impedance of 50Ω. Therefore, an impedance matching pad with a bandwidth of 2 GHz (Fairview Microwave-SI 1560) is used in the design for the demonstration of 4K video transmission. To our knowledge, currently, this is the only commercially available impedance matching pad with BNC to SMA connectors that offers broadband operation.
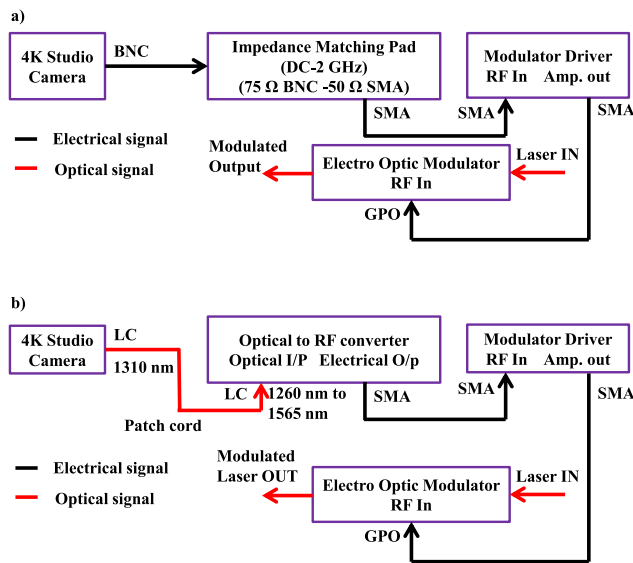

FIGURE 11. Block diagram for the integration of a 4K video camera with transmitter of the THz communication system using a) electrical and b) optical signal output from the camera.

However, due to 2 GHz bandwidth limitation of the impedance matching circuit, we find that transmission of the uncompressed 4K video is limited to 30 fps (∼6 Gbps). While feeding the video signal from the camera to the optical modulator, the control settings (amplified RF voltage level and modulator bias voltage) for RF amplifier and the external modulator are kept similar to the BER measurements.

Alternatively, in Fig.11 (b) we present integration of a 4K camera with THz transmitter when using optical signal from the camera output. In order to use optical video signal

with the THz transmitter, it has to be converted to electrical signal to feed the optical modulator. Therefore, an optical transceiver (Finisar-FTLX1471D3BCL) which is integrated with the test equipment (Anritsu-Mp2100B) is used for the optical to electrical conversion. The optical signal from the 4K camera was carried via a single mode fiber. The electrical output of the optical transceiver features SMA connector with 50Ω impedance, which was then connected to the SMA input RF port of the optical modulator driver. Using both designs presented in Fig.11, an uncompressed 4K video up to 30 fps can be transmitted. The advantage of using electrical output from the camera (Fig.10 (a)) is that, the impedance matching pad is compact, less expensive and does not require the power supply for the operation. However, the RF cable is bulky to handle and suffers from high signal loss as the length increases. Conversely, while using optical output from the camera (Fig.11 (b)), we benefit from low losses of the optical fiber and it also supports large bandwidth of the baseband video signal. At the same time, the maximum data rate of the optical transmitter supported by the 4K camera is 6 Gbps, limiting the uncompressed 4K video frame rate to 30 fps. For our demonstration, we used the optical signal from the 4K camera to integrate with the THz transmitter (Fig.11, b) as it favors easy handling and integration using plug-in connectors.

While so far, we have discussed transmitter side of the THz communication system for video transmission, we now focus on the receiver side. At the receiver side, in order to present and analyze the transmitted video, we have explored two options including a 4K-capable display (ASUS-MG28UQ), and a 4K-capable video receiver (Blackmagic) and a storage unit. The received, demodulated and amplified electrical signal is converted into optical signal using optical transceiver of the Anritsu-MP2100B test equipment for further processing as shown in Fig.12. It is possible to use the impedance matching pad (similar to the transmitter integration) after the LNA without converting it to the optical signal to connect it to the computer interface card. But, the high frequency components (>2 GHz) present in the baseband signal will be filtered by the impedance matching pad (Bandwidth: DC-2 GHz), which is not favorable in signal reconstruction. Therefore,
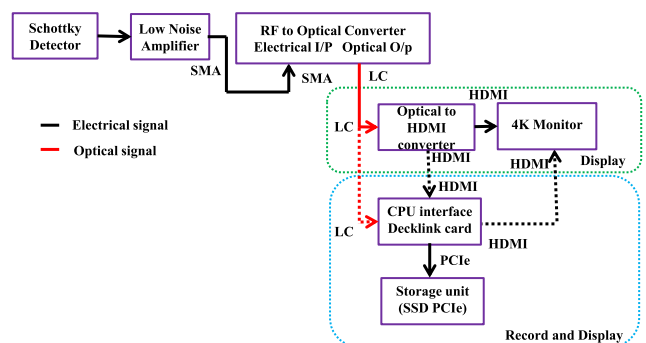

FIGURE 12. Block diagram for the receiving, visualization and recording of the transmitted uncompressed HD and 4K video.

we preferred to use the optical conversion as the fiber can carry all the frequency components present in the amplified baseband signal, favoring efficient signal reconstruction and easy handling. Particularly, the electrical to optical conversion corrects the amplitude distortions that are present in the electrical signals (see the eye pattern in Fig.13).
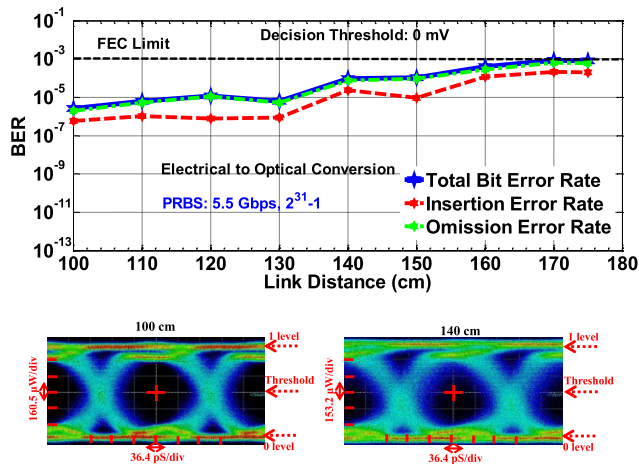

FIGURE 13. Measured BER after converting electrical output signal of LNA to optical signal and then again to electrical signal (Fixed decision Threshold: 0 mV). The eye diagram is recorded after converting electrical output signal of LNA to optical.

The receiver configuration presented in Fig.12 can be modified depending on the end requirement (display or record). If displaying the 4K video is the only requirement, an optical to HDMI converter (Blackmagic-Teranex Mini Optical Fiber) is used. A high-speed computer interface card (Blackmagic-Decklink 4K Extreme 12G) is employed when both recording and displaying the 4K video simultaneously is required. The computer interface card supports SDI (electrical), HDMI and optical input/output interfaces allowing to record the received uncompressed video signal on the solid state hard drive (SSD). In order to test the capability of the SSD to record uncompressed video signals, we first analyzed the writing and reading speed of the SSD with PCIe 3.0 interface (SAMSUNG-960 PRO M.2 2 TB NVMe PCIe 3.0) and SSD with SATA interface (SAMSUNG-MZ75E500) using Black-magic disk speed test software. Particularly, we connected four SSD's (500 GB each) with SATA interface using RAID 0 configuration to increase the data transfer speed. The analysis showed that it is possible to write and read 2000 MB/s using SSD with PCIe3.0 interface whereas, the data transfer speed of the SSD with SATA interface is slower (Writing speed: 1197.4 MB/s and Reading: 1473.2 MB/s). Therefore, we used the SSD with PCIe3.0 interface to record the uncompressed HD and 4K video.

Before performing the video transmission experiment, the BER measurement is conducted again using PRBS data in order to compare whether the total BER after electrical (output of LNA) to optical conversion is similar to the total BER measured before conversion. Since, the BER can be measured only for the electrical signals in our test equipment,

the optical signal is further converted to electrical signal using optical transceiver (only for BER measurements in this case). The BER measurement is conducted at several link distances with fixed decision threshold (0 mV) as shown in Fig.13. However, the eye pattern in the inset of Fig.13 is measured for optical signal. We observe that the total BER after optical conversion is slightly increased when compared to the BER that is measured with the electrical signal after LNA (Fig.10 (a)). Therefore, we conclude that the effect of converting the electrical signal to optical signal for the video transmission experiment is negligible.

For the demonstration of video transmission wirelessly, an uncompressed HD (1920 x 1080 at 60 fps) and 4K (3840 x 2160 at 30 fps) videos are transmitted individually through the THz communication system at the carrier frequency of 138 GHz. The corresponding data rates are 2.97 Gbps and 5.94 Gbps for HD and 4K video respectively. For the ease of analysis, the received video is recorded as image data (Digital Picture Exchange format) where individual frame from the video is recorded as an image. The received frames are recorded at a given link distance for a duration of 30 minutes. We analyzed only the synchronization errors in this work by analyzing the black frames. Although the clarity of the video is not visually degraded except the black frames, a standard metrics may be applied to validate the quality of the received video. However, analysis of full frame requires both video signals (video signal directly from the camera and the video signal after wireless reception) need to be recorded at the same time for better comparison which is beyond the scope of this paper. Therefore, we limited our experiments by studying the black frames (synchronization error) only. The number of black frames is identified by taking the small portion (5x5 pixels) in each frame and analyzing the average RGB value. The RGB value of the black frame is zero and therefore any frame that is having the average RGB value above this threshold is identified as a valid frame.

The black frame is a tool to measure the performance of the wireless streaming which is caused due to the error in the synchronization packets. The timing synchronization of the digital video is provided by the End of Active Video (EAV) and Start of Active Video (SAV) sequences with a unique hexadecimal word pattern. The hexadecimal word pattern refers to 3FF (all bits are 1), 000 (all bits are 0), 000 (all bits are 0), and XYZ (10-bit word). The XYZ of a 10-bit word corresponds to bit number 8,7 and 6 which is used to indicate whether the video scanning is progressive or interlaced, active video or blanking interval and EAV or SAV respectively. Therefore, any error in this synchronization packet leads to the black frame. The identified black frames for the HD (60 fps) and 4K (30 fps) video which is recorded at the link distance of 30 cm for the duration of 30 minutes (HD-108000 frames and 4K-54000 frames) is shown in Fig.14. We see that the possibility of black frame is higher for 4K video transmission when compared with the HD video due to minor instability of the THz communication system during the measurement duration.
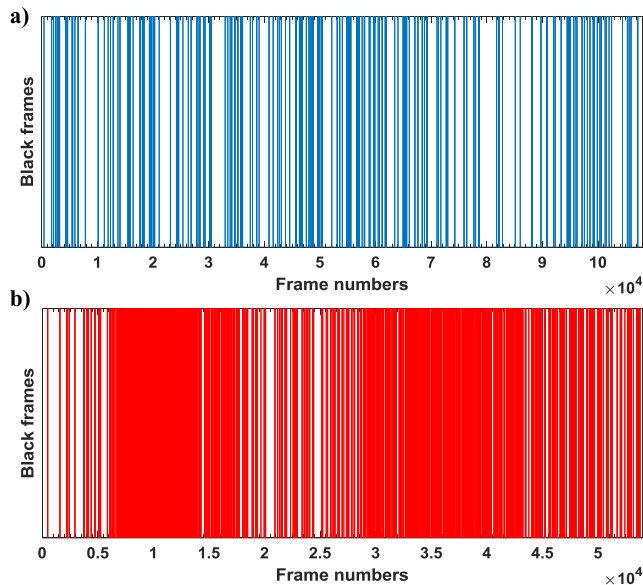
FIGURE 14. Identified black frames which is recorded for 30 minutes at a link distance of 30 cm. a) HD video (60 fps) and b) 4K video (30 fps).
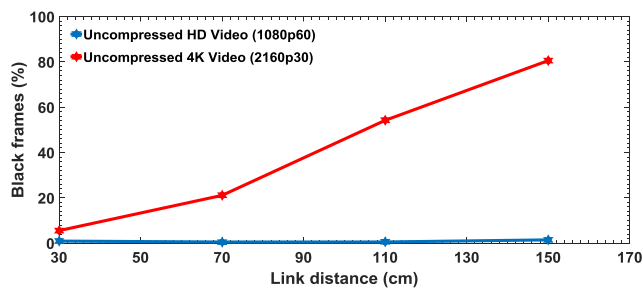

FIGURE 15. Percentage of black frames for HD and 4K video as a function of link distance.

We also did the similar experiment by increasing the wireless link distance and the percentage of black frames is calculated for both HD and 4K videos as shown in Fig.15. We see that, the percentage of black frames is less than 0.5% for HD video and ~5% for 4K video at the link distance of 30 cm. By increasing the link distance, the percentage of black frames is almost constant for HD video but increases for 4K video. It indicates that the probability of errors in the timing synchronization packets is higher for the 4K video due to high bit error rate.

VI. CONCLUSION

To conclude, we showed the design and evaluated the performance of a photonics based THz wireless communication system that is built using all commercially available system components. Two independent tunable lasers operating in the infrared C-band are used as the source for the generation of THz carrier wave in the photomixer. A zero bias Schottky diode is used as the detector and demodulator followed by a high gain and low noise amplifier. The optimum carrier frequency (138 GHz) is chosen by analyzing the THz output

power and the responsivity of commercially available ZBDs. The performance of the built system is evaluated by measuring the BER for the PRBS data at the bit rate of 5.5 Gbps. By optimizing the decision threshold, an error-free data transmission is achieved at a link distance of 1 m. As a practical demonstration, we detailed the integration of a 4K camera at the THz transmitter and the video receiver electronics at the THz receiver. We showed the successful transmission of uncompressed HD and 4K video. The link quality for the video transmission is analyzed and the percentage of black frames is measured. It is observed that the percentage of black frames is higher for the transmitted uncompressed 4K video due to the high bit errors at the increased link distance, whereas ~99% of the uncompressed HD video is received successfully. The obtained results confirm that it is now possible to realize a short-range high-quality video transmission using THz wireless communication system for commercial applications. Finally, we also discussed about several methods for increasing the link distance and data rate along with the potential academic and industrial applications of the proposed system.

REFERENCES

[1] *The Zettabyte Era: Trends and Analysis*, Cisco, San Jose, CA, USA, Jul. 2017.

[2] T. Kürner and S. Priebe, "Towards THz communications—Status in research, standardization and regulation," *J. Infr., Millim., Terahertz Waves*, vol. 35, no. 1, pp. 53–62, 2014.

[3] Y. Niu, Y. Li, D. Jin, L. Su, and A. V. Vasilakos, "A survey of millimeter wave communications (mmWave) for 5G: Opportunities and challenges," *Wireless Netw.*, vol. 21, no. 8, pp. 2657–2676, 2015.

[4] J. Zhang, P. Tang, L. Tian, Z. Hu, T. Wang, and H. Wang, "6–100 GHz research progress and challenges from a channel perspective for fifth generation (5G) and future wireless communication," *Sci. China Inf. Sci.*, vol. 60, no. 8, p. 080301, 2017.

[5] I. F. Akyildiz, J. M. Jornet, and C. Han, "TeraNets: Ultra-broadband communication networks in the terahertz band," *IEEE Wireless Commun.*, vol. 21, no. 4, pp. 130–135, Aug. 2014.

[6] I. F. Akyildiz, J. M. Jornet, and C. Han, "Terahertz band: Next frontier for wireless communications," *Phys. Commun.*, vol. 12, pp. 16–32, Sep. 2014.

[7] M. A. Akkas, "Terahertz wireless data communication," *Wireless Netw.*, pp. 1–11, 2017.

[8] International Telecommunication Union, "Technology trends of active services in the frequency range 275–3000 GHz," Int. Telecommun. Union, Geneva, Switzerland, Tech. Rep. SM.2352-0 (06/2015). Accessed: Jun. 6, 2018. [Online]. Available: https://www.itu.int/dms_pub/itu-r/opb/rep/R-REP-SM.2352-2015-PDF-E.pdf

[9] Asia–Pacific Telecommunity, "APT report on technology trends of telecommunications above 100 GHz," Asia–Pacific Telecommunity, Bangkok, Thailand, Tech. Rep. ASTAP/REPT 4 (ASTAP19, Manila, 2011). Accessed: Jun. 6, 2018. [Online]. Available: https://www.apt.int/sites/default/files/Upload-files/ASTAP/Rept-4-Technology%20Trends%20above%20100GHz.pdf

[10] International Telecommunication Union, M.2417-0 (11/2017), "Technical and operational characteristics of land-mobile service applications in the frequency range 275–450 GHz." Accessed: Jun. 6, 2018. [Online]. Available: https://www.itu.int/dms_pub/itu-r/opb/rep/R-REP-M.2417-2017-PDF-E.pdf

[11] A. Hirata *et al.*, "120-GHz-band wireless link technologies for outdoor 10-Gbit/s data transmission," *IEEE Trans. Microw. Theory Techn.*, vol. 60, no. 3, pp. 881–895, Mar. 2012.

[12] H. Takahashi, A. Hirata, J. Takeuchi, N. Kukutsu, T. Kosugi, and K. Murata, "120-GHz-band 20-Gbit/s transmitter and receiver MMICs using quadrature phase shift keying," in *Proc. IEEE 7th Eur. Microw. Integr. Circuits Conf. (EuMIC)*, Oct. 2012, pp. 313–316.

[13] A. Hirata *et al.*, "5.8-km 10-Gbps data transmission over a 120-GHz-band wireless link," in *Proc. IEEE Int. Conf. Wireless Inf. Technol. Syst. (ICWITS)*, Aug./Sep. 2010, pp. 1–4.

[14] H. Takahashi, T. Kosugi, A. Hirata, K. Murata, and N. Kukutsu, "10-Gbit/s quadrature phase-shift-keying modulator and demodulator for 120-GHz-band wireless links," *IEEE Trans. Microw. Theory Techn.*, vol. 58, no. 12, pp. 4072–4078, Dec. 2010.

[15] T. Nagatsuma, G. Ducournau, and C. C. Renaud, "Advances in terahertz communications accelerated by photonics," *Nature Photon.*, vol. 10, pp. 371–379, May 2016.

[16] I. Mehdi, J. V. Siles, C. Lee, and E. Schlecht, "THz diode technology: Status, prospects, and applications," *Proc. IEEE*, vol. 105, no. 6, pp. 990–1007, Jun. 2017.

[17] H. Shams and A. Seeds, "Photonics, fiber and THz wireless communication," *Opt. Photon. News*, vol. 28, no. 3, pp. 24–31, 2017.

[18] A. J. Deninger, A. Roggenbuck, S. Schindler, and S. Preu, "2.75 THz tuning with a triple-DFB laser system at 1550 nm and InGaAs photomixers," *J. Infr., Millim., Terahertz Waves*, vol. 36, no. 3, pp. 269–277, 2015.

[19] H. Ito and T. Ishibashi, "Photonic terahertz-wave generation using slot-antenna-integrated uni-traveling-carrier photodiodes," *IEEE J. Sel. Topics Quantum Electron.*, vol. 23, no. 4, Jul./Aug. 2017, Art. no. 3800907.

[20] I. Morohashi *et al.*, "Terahertz source with broad frequency tunability up to 3.8 THz using MZ-FCG for frequency reference in phase-locking of THz source devices," in *Proc. IEEE Int. Topical Meeting Microw. Photon. (MWP)*, Oct./Nov. 2016, pp. 126–128.

[21] T. Ishibashi, Y. Muramoto, T. Yoshimatsu, and H. Ito, "Unitraveling-carrier photodiodes for terahertz applications," *IEEE J. Sel. Topics Quantum Electron.*, vol. 20, no. 6, Nov./Dec. 2014, Art. no. 3804210.

[22] T. Nagatsuma and H. Ito, "High-power RF uni-traveling-carrier photodiodes (UTC-PDs) and their applications," in *Advances in Photodiodes*. Rijeka, Croatia: InTech, 2011.

[23] T. Umezawa *et al.*, "Bias-free operational UTC-PD above 110 GHz and its application to high baud rate fixed-fiber communication and W-band photonic wireless communication," *J. Lightw. Technol.*, vol. 34, no. 13, pp. 3138–3147, Jul. 1, 2016.

[24] E. Peytavit *et al.*, "Milliwatt-level output power in the sub-terahertz range generated by photomixing in a GaAs photoconductor," *Appl. Phys. Lett.*, vol. 99, no. 22, p. 223508, 2011.

[25] H. J. Song, K. Ajito, Y. Muramoto, A. Wakatsuki, T. Nagatsuma, and N. Kukutsu, "Uni-travelling-carrier photodiode module generating 300 GHz power greater than 1 mW," *IEEE Microw. Wireless Compon. Lett.*, vol. 22, no. 7, pp. 363–365, Jul. 2012.

[26] T. Nagatsuma *et al.*, "Terahertz wireless communications based on photonics technologies," *Opt. Express*, vol. 21, nos. 20, pp. 23736–23747, Sep. 2013.

[27] T. Nagatsuma and G. Carpintero, "Recent progress and future prospect of photonics-enabled terahertz communications research," *IEICE Trans. Electron.*, vol. E98-C, no. 12, pp. 1060–1070, 2015.

[28] H. Shams, M. J. Fice, K. Balakier, C. C. Renaud, F. V. Dijk, and A. J. Seeds, "Photonic generation for multichannel THz wireless communication," *Opt. Express*, vol. 22, no. 19, pp. 23465–23472, Sep. 2014.

[29] S. Koenig *et al.*, "Wireless sub-THz communication system with high data rate," *Nature Photon.*, vol. 7, no. 12, pp. 977–981, 2013.

[30] G. Ducournau *et al.*, "Ultrawide-bandwidth single-channel 0.4-THz wireless link combining broadband quasi-optic photomixer and coherent detection," *IEEE Trans. Terahertz Sci. Technol.*, vol. 4, no. 3, pp. 328–337, May 2014.

[31] X. Yu *et al.*, "60 Gbit/s 400 GHz wireless transmission," in *Proc. IEEE Int. Conf. Photon. Switching (PS)*, Sep. 2015, pp. 4–6.

[32] X. Yu *et al.*, "160 Gbit/s photonics wireless transmission in the 300–500 GHz band," *APL Photon.*, vol. 1, no. 8, p. 081301, 2016.

[33] S. Diebold *et al.*, "High-speed error-free wireless data transmission using a terahertz resonant tunnelling diode transmitter and receiver," *Electron. Lett.*, vol. 52, no. 24, pp. 1999–2001, 2016.

[34] T. Nagatsuma, K. Oogimoto, Y. Inubushi, and J. Hirokawa, "Practical considerations of terahertz communications for short distance applications," *Nano Commun. Netw.*, vol. 10, pp. 1–12, Dec. 2016.

[35] J. Ma, N. J. Karl, S. Bretin, G. Ducournau, and D. M. Mittleman, "Frequency-division multiplexer and demultiplexer for terahertz wireless links," *Nature Commun.*, vol. 8, no. 1, p. 729, Sep. 2017.

[36] S. Blin *et al.*, "Wireless communication at 310 GHz using GaAs high-electron-mobility transistors for detection," *J. Commun. Netw.*, vol. 15, no. 6, pp. 559–568, 2013.

[37] Q. Wu *et al.*, "A 21 km 5 Gbps real time wireless communication system at 0.14 THz," in *Proc. IEEE 42nd Int. Conf. Infr., Millim., Terahertz Waves (IRMMW-THz)*, Aug./Sep. 2017, pp. 1–2.

[38] G. Ducournau *et al.*, "High-definition television transmission at 600 GHz combining THz photonics hotspot and high-sensitivity heterodyne receiver," *Electron. Lett.*, vol. 50, no. 5, pp. 413–415, Feb. 2014.

[39] T. M. Narytnyk, "Possibilities of using THz-band radio communication channels for super high-rate backhaul," *Telecommun. Radio Eng.*, vol. 73, no. 15, pp. 1361–1371, 2014.

[40] D. Bojic *et al.*, "Advanced wireless and optical technologies for small-cell mobile backhaul with dynamic software-defined management," *IEEE Commun. Mag.*, vol. 51, no. 9, pp. 86–93, Sep. 2013.

[41] P. T. Dat, A. Kanno, K. Inagaki, and T. Kawanishi, "High-capacity wireless backhaul network using seamless convergence of radio-over-fiber and 90-GHz millimeter-wave," *J. Lightw. Technol.*, vol. 32, no. 20, pp. 3910–3923, Oct. 15, 2014.

[42] V. Petrov, A. Pyattaev, D. Moltchanov, and Y. Koucheryavy, "Terahertz band communications: Applications, research challenges, and standardization activities," in *Proc. IEEE 8th Int. Congr. Ultra Mod. Telecommun. Control Syst. Workshops (ICUMT)*, Oct. 2016, pp. 183–190.

[43] (2015). *4K Technology Market Worth $102.1 Billion by 2020*. Accessed: Jun. 10, 2018. [Online]. Available: http://www.marketsandmarkets.com/PressReleases/4k-technology.asp and http://marketsandmarkets.com

[44] D. Mirzoev. (2014). "Wireless transmission of video for biomechanical analysis." [Online]. Available: https://arxiv.org/abs/1404.2343

[45] M. C. Batistatos, G. V. Tsoulos, and G. E. Athanasiadou, "Mobile telemedicine for moving vehicle scenarios: Wireless technology options and challenges," *J. Netw. Comput. Appl.*, vol. 35, no. 3, pp. 1140–1150, 2012.

[46] T. Toma, S. Suzuki, H. Tokura, Y. Inaba, T. Ogi, and A. Y. Koike, "Evaluation of 4K ultra definition video for telemedicine—Possibility of teledermatology applications," *Jpn. J. Telemed. Telecare*, vol. 9, no. 2, pp. 66–73, 2013.

[47] Y. Miki *et al.*, "Readying for UHDTV broadcasting in Japan," *SMPTE Motion Imag. J.*, vol. 126, no. 2, pp. 46–52, 2017.

[48] D. Stanze, A. Deninger, A. Roggenbuck, S. Schindler, M. Schlak, and B. Sartorius, "Compact cw terahertz spectrometer pumped at 1.5 μm wavelength," *J. Infr., Millim., Terahertz Waves*, vol. 32, no. 2, pp. 225–232, Feb. 2011.

[49] S. Nellen, B. Globisch, R. B. Kohlhaas, L. Liebermeister, and M. Schell, "Recent progress of continuous-wave terahertz systems for spectroscopy, non-destructive testing, and telecommunication," *Proc. SPIE*, vol. 10531, p. 105310C, Feb. 2018.

[50] B. Globisch *et al.*, "Absolute terahertz power measurement of a time-domain spectroscopy system," *Opt. Lett.*, vol. 40, no. 15, pp. 3544–3547, 2015.

[51] P. H. Siegel, "Terahertz technology," *IEEE Trans. Microw. Theory Techn.*, vol. 50, no. 3, pp. 910–928, Mar. 2002.

[52] X. Li, J. Yu, J. Zhang, Z. Dong, F. Li, and N. Chi, "A 400G optical wireless integration delivery system," *Opt. Express*, vol. 21, no. 16, pp. 18812–18819, 2013.

[53] M. J. Fice *et al.*, "146-GHz millimeter-wave radio-over-fiber photonic wireless transmission system," *Opt. Express*, vol. 20, no. 2, pp. 1769–1774, 2012.

[54] G. Ducournau *et al.*, "Coherent THz communication at 200 GHz using a frequency comb, UTC-PD and electronic detection," *Electron. Lett.*, vol. 50, no. 5, pp. 386–388, Feb. 2014.

KATHIRVEL NALLAPPAN received the B.E. degree in electronics and communication engineering and the M.Tech. degree in laser and electro-optical engineering from Anna University, Tamil Nadu, India, in 2010 and 2013, respectively. He was a Senior Project Fellow with the Structural Engineering Research Center, India, for a period of one year, he joined as a Research Intern with the Research Group of Prof. M. Skorobogatiy, Polytechnique Montréal, Canada. He is currently pursuing the Ph.D. degree in Terahertz communications with Polytechnique Montréal. His research interest includes Terahertz and infrared free space communications, waveguide modeling, Terahertz spectroscopy, and imaging.

HICHEM GUERBOUKHA received the B.Sc. degree in engineering physics and the M.Sc. degree in applied science from Polytechnique Montréal, Montreal, QC, Canada, in 2014 and 2015, respectively, where he is currently pursuing the Ph.D. degree in THz computational imaging. His research interests include THz instrumentation and waveguides, THz communications, and THz computational imaging. He was a recipient of the Etoile Student-Researcher from Fonds de recherche–Nature et technologies in 2015 and the Best M.S. Thesis Prize from Polytechnique Montréal.

CHAHÉ NERGUIZIAN (M'00) received the B.Eng. degree from Polytechnique Montréal in 1981, the M.Eng. degree from McGill University in 1983, and the Ph.D. degree the Université du Québec in 2003, all in electrical engineering. After two years of industrial experience as a Microwave Engineer with the Avionic Division, Canadian Marconi, Canada, he joined with the Department of Electrical and Computer Engineering, Polytechnique Montréal, in 1986. Since 2007, he has been the Head of the Telecommunication and Microwave Section, Electrical Engineering Department. He is currently a Full Professor with the Telecommunication Group. His research interests are in wireless radio propagation (narrow band, wide band, and ultra wide band channel characterization), indoor-outdoor radiolocation (RFID and WLAN) and advanced wireless communication (OFDM, MIMO, and UWB). He is a member of the Order of Engineers of Quebec.

MAKSIM SKOROBOGATIY received the M.Sc. degree in Electrical Engineering and Computer Science from MIT in 2000, and the Ph.D. degree in physics from MIT in 2001. He then served with the MIT spin-off Omniguide Inc., where he was involved in the development of hollow-core fibers for guidance of high-power mid-IR laser beams. He has been a professor of engineering physics with Polytechnique Montréal since 2003. M. Skorobogatiy was awarded the Tier 2 Canada Research Chairs in micro and nano-photonics in 2005, and 2010, while in 2016 he was awarded a Tier 1 Canada Research Chair in ubiquitous THz photonics. The support from the Canada Research Chairs program allowed him to pursue many high-risk exploratory projects in guided optics, smart materials, and recently THz photonics, which have resulted in significant contributions in these booming research fields. In 2017, he was elected to the fellow of the Optical Society of America for his pioneering contributions to the development of micro-structured and photonic crystal multi-material fibers and their applications to light delivery, sensing, smart textiles, and arts. The same year, he was also promoted to the Senior Member of the IEEE for his contribution in engineering and applied research. In 2012, he was awarded the rank of a Professional Engineer by the Order of Engineers of Quebec, Canada.

• • •